Development and Characterization of Composite YSZ-PEI Electrophoretically Deposited Membrane for Li-Ion Battery

ARTICLE *in* THE JOURNAL OF PHYSICAL CHEMISTRY B · JULY 2012

Impact Factor: 3.3 · DOI: 10.1021/jp305087h · Source: PubMed

8 AUTHORS, INCLUDING:

D. Golodnitsky
Tel Aviv University
94 PUBLICATIONS **2,704** CITATIONS
SEE PROFILE

Hadar Mazor
Tel Aviv University
7 PUBLICATIONS **136** CITATIONS
SEE PROFILE

Zahava Barkay
Tel Aviv University
93 PUBLICATIONS **1,335** CITATIONS
SEE PROFILE

E. Peled
Tel Aviv University
170 PUBLICATIONS **5,350** CITATIONS
SEE PROFILE

THE JOURNAL OF PHYSICAL CHEMISTRY B

Article

pubs.acs.org/JPCB

Development and Characterization of Composite YSZ–PEI Electrophoretically Deposited Membrane for Li-Ion Battery

R. Hadar,*[,†] D. Golodnitsky,*[,†,‡] H. Mazor,[†] T. Ripenbein,[†] G. Ardel,[†] Z. Barkay,[‡] A. Gladkich,[‡] and E. Peled[†]

[†]School of Chemistry, [‡]Wolfson Applied Materials Research Center, Tel Aviv University, Tel Aviv 69978, Israel

ABSTRACT: In this work, the electrophoretic-deposition (EPD) method was used to fabricate pristine and composite ceramic–polymer membranes for application in planar and 3D microbattery configurations. The major focus was on the effect of polyethyleneimine additive on the morphology, composition, and electrochemical properties of the membrane. The ionic conductivity, cycleability, and charge/discharge behavior of planar $LiFePO_4$/Li cells comprising composite porous YSZ-based membrane with impregnated $LiPF_6$ EC:DEC electrolyte were found to be similar to the cells with commercial Celgard membrane. Conformal EPD coating of the electrode materials by a thin-film ceramic separator is advantageous for high-power operation and safety of batteries.

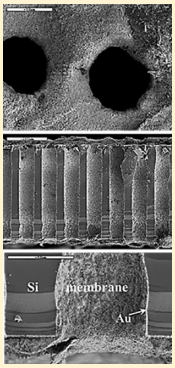

INTRODUCTION

The first commercial rechargeable Li-ion battery was constructed by Sony in 1991. The energy density, number of charge/discharge cycles, and shelf life of the Li-ion battery is better than other secondary batteries, and this led to considerable investment in the development and production of this battery. Today, Li-ion is the preferred battery for small-scale electronics and electric and hybrid vehicles and is expected to make inroads in the power-tools market.[1−3] However, the miniaturization of electronic components has not been accompanied by a similar achievement in the field of power sources, and there is a strong demand for smaller batteries with higher energy density and greater power capabilities.

One of the developments aimed at meeting these requirements is a three-dimensional thin-film microbattery (3DMB). The common requirement of the 3DMB is that ion-diffusion distance will remain short and one-dimensional (or nearly so) at the microscopic level, while the electrodes are configured in complex geometries (i.e., nonplanar) in order to increase the energy density and power density of the cell within the footprint area.[4−8]

We have recently developed methods of creating a thin-film Li-ion 3D microbattery on a perforated silicon substrate, with high-aspect-ratio microchannels.[6−8] 3D microbatteries comprise a nickel or gold current collector, a cathode (MoO_xS_{2-x}, FeO_xS_y, V_2O_5, or $LiFePO_4$), a hybrid-polymer electrolyte (HPE), and an anode (graphite, lithiated graphite, or $LiTiO_2$). All the layers, except for the anode, are thin conformal films, formed in such a way that they follow the contours of all available hollow surfaces of the perforated substrate.[6−8] This battery architecture provides an increase of more than an order of magnitude in the surface area available for active cathode and anode materials, over the original substrate footprint. In addition, since the weight of a perforated substrate is only a fraction of that of the full substrate (typically 20−30%), the specific gravimetric capacity and energy are further increased by a factor of 5−10. However, another major advantage over conventional/commercial planar thin-film microbatteries is expressed by the much larger currents provided by this 3D microbattery, which result from the extremely large surface areas of nanograin electrode materials and contact areas between the active layers and the central electrolyte layer.

A great challenge lays in the achievement of conformal deposition of all the battery-building materials on the complex-geometry electrodes with the use of simple and inexpensive electrochemical methods. Special attention was given to the cell separator (an ion-conducting membrane), since it must have the appropriate electrochemical properties in addition to the mechanical properties needed to withstand the pressures of anode insertion, sealing of the cell, and changes in the electrode volumes during the operation of the cell.

A conventional separator is usually a microporous polyolefin such as a polypropylene Celgard membrane. The drawbacks of this brand of separators are their poor thermal and mechanical integrity—the polymer will soften or melt when the temperature reaches 130 °C or higher, and this leads to shrinkage or possible internal short circuits due to lithium dendrites.[1−3,9]

Inorganic ceramic materials have very good thermal and mechanical properties with excellent wettabilty and have been

Special Issue: Electrophoretic Deposition

Received: May 25, 2012
Revised: July 17, 2012
Published: July 18, 2012

dx.doi.org/10.1021/jp305087h | J. Phys. Chem. B 2013, 117, 1577−1584

widely used as additives to modify polymeric separators to improve these qualities. A separator composed of inorganic materials as the main component with some polymeric binder has been developed,[9−12] but this class of separators is not sufficiently elastic to withstand the common Li-ion cell-winding procedure. Since most microbatteries and 3DMB designs do not require winding, inorganic separators present a good choice. However, conventional fabrication techniques such as casting or spin-coating are not suitable for the conformal deposition of membranes on complicated electrode geometries.

This work describes the development and characterization of yttria-stabilized zirconia (YSZ)−polyethyleneimine (PEI) composite membrane prepared by electrophoretic deposition (EPD), for 3D microbatteries assembled on perforated silicon. The most common use of EPD is in the production of ceramic components. EPD has gained significant interest because of the high versatility of its use with different materials including nanoparticles and its cost-effectiveness, as it requires only simple equipment. EPD provides good conformal deposits on complicated geometries,[13−18] and the YSZ ceramics ensure excellent electrical isolation, thermal stability, good wettability, and high mechanical integrity.

This paper encompasses analysis of the deposition process, morphology, chemical composition, and electrochemical characterization of the electrophoretically deposited planar and 3D YSZ−PEI membrane.

EXPERIMENTAL SECTION

The deposition bath for EPD was prepared by the following procedure: 0.7 g of yttria-stabilized zirconia powder (YSZ- 8% Yttria Sigma Aldrich) was dispersed in 150 mL of ethanol (Frutarom 99.5%). A 0.4 mL portion of acetylacetone (Fluka 99.5%) was added, and the solution was stirred with a magnetic stirrer for 15 h in a closed vessel. A second solution containing 100 mL of ethanol, 4 mL of acetone (Fluka 99.5%), 2 mL of deionized water (18.2 MΩ), and 0.0027 g of I_2 was prepared just before deposition and stirred for 20 min. The YSZ suspension was added to the second solution, and the mixture was sonicated for 20 min in an ultrasonic bath containing ice. This procedure is similar to that developed by Grinis et al. for the deposition of TiO_2.[19,20] The procedure was modified by replacing TiO_2 with YSZ which has the high electrical resistivity needed for battery separators and adding PEI as a polymer binder and lithium-ion-conducting medium. Polyethyleneimine (PEI- Fluka 50%(w/v) in H_2O, M_n = 60000, M_w = 750000) was used, since the binder-free films were too brittle and sintering is not an option, since current-collector and battery-electrode materials cannot withstand the temperatures exceeding 1000 °C typically used for YSZ sintering. The PEI addition was performed as follows: PEI 50%(w/v) (50 g/100 mL) in H_2O solution was diluted with ethanol to a concentration of 8.33 g/L. Then, 1.26 mL of the diluted solution was added to the EPD suspension, which underwent the ultrasonic treatment, and was then stirred for 1 h before deposition. The net weight of PEI added is 0.0105 g which is 1.5% (w/w) of the 0.7 g YSZ powder used. The amount of water introduced by dissolved PEI is less than 0.5% of the total volume of solvents in the EPD suspension, so it can be assumed that there is no significant concentration change. The final pH of the suspension was about 4.5.

A Keithley SourceMeter, model 2400, interfaced with LabTracer software and a PC, was used to control the EPD process and to monitor the current and voltage profiles.

Deposition of the YSZ separator on planar substrates (working electrode) was performed on pristine nickel disks and nickel coated by $LiFePO_4$ (LFP) composite cathodes with the use of a graphite plate as counter electrode. The LFP films were electrophoretically deposited by a procedure described elsewhere.[22] Deposition of the membrane on 3D gold-coated perforated silicon[7] was performed with the use of a flow system. The gold-coated silicon was used as a working electrode between two squares of platinum gauze. The distance between working and counter electrodes was 1.5 cm.

Samples for electrochemical-cycling tests were dried under a vacuum for 15 h at 115 °C, and transferred to an argon-filled glovebox (Brown, ≤10 ppm water) for cell assembly. Cycling performance was tested with the use of 2032 coin cells comprising 0.2 cm^2 lithium−metal anode, YSZ membrane deposited on LFP cathodes, and soaked in 1 M $LiPF_6$ 1:1 EC:DEC electrolyte. Tests were carried out at room temperature in a Maccor series 2000 battery-test system.

Electrochemical-impedance spectroscopy was used to test membrane conductivity.

Conductivity cells (in the coin-cell 2032 setup) comprise a YSZ membrane deposited on a nickel disk, 0.57 cm^2 lithium−metal anode, and 1 M $LiPF_6$ 1:1 EC:DEC electrolyte. Tests were carried out at room temperature with a Solartron Impedance Analyzer 1260 with 20 mV amplitude and a frequency range of 5 MHz to 1 Hz. A Celgard commercial separator was used as a reference, and baseline liquid-electrolyte-conductivity values were taken from ref 1.

Surface morphology was studied with a JSM-6300 scanning microscope (Jeol Co.) and a Veeco Dektak 6 m stylus profilometer. TOFSIMS tests were performed under the following operating conditions: In^+ primary ions and beam diameter of 1 μm with the use of TRIFT II (Physical Electronics Inc., USA).

Samples for simultaneous TGA−DTA were transferred from the glovebox in a sealed vessel just before each measurement. The sample compartment was flushed with dried UHP argon at all times. The TGA tests were carried out with a TA-Instruments module SDT 2960. TGA−DTA runs were recorded at a scan rate of 10° min^{-1} up to 500 °C.

RESULTS AND DISCUSSION

Electrophoretic deposition (EPD) is a two-step process in which charged particles, suspended in a liquid medium, migrate under an electric field and deposit on (adhere to) the electrode with opposite charge. The difference between EPD and electrolytic deposition (ELD) is that, while in ELD, the moving species are ions that will eventually be part of the chemical reaction on the electrode surface, in the EPD process, the moving particles are present as a powder suspended in the solution. Particle size can vary from a few nanometers to several micrometers. The particles are usually charged by the adsorption of ions from the solution and do not take part in the redox reactions.

Although aqueous solvents can be used in the electrophoretic process, nonaqueous solvents are often selected because aqueous solvents evolve hydrogen and oxygen, which causes the formation of pores in the deposits and their embrittlement following electrolysis of water.

A suspension for EPD is a complex system in which each component has a substantial effect on the deposition efficiency, morphology, and density of the film.

dx.doi.org/10.1021/jp305087h | J. Phys. Chem. B 2013, 117, 1577−1584

In cathodic deposition from nonaqueous solutions, the particles can be charged by the adsorption of protons, which are generated by the keto−enol reactions 1−4 of acetone and acetylacetone.[14,26]

$$CH_3COCH_3 \leftrightarrow CH_3C(OH)CH_2 \quad (1)$$

$$CH_3C(OH)CH_2 + I_2 \rightarrow CH_2COCH_2I + H^+ + I^- \quad (2)$$

$$CH_3COCH_2COCH_3 \leftrightarrow CH_2C(OH)CH_2C(OH)CH_2 \quad (3)$$

$$CH_2C(OH)CH_2C(OH)CH_2 + 2I_2 \rightarrow ICH_2COCH_2COCH_2I + 2H^+ + 2I^- \quad (4)$$

This method, in which the acetylacetone was added to the solution, has been discussed by Grinis et al.[19] The authors suggest that, in addition to the generation of protons, adsorption of acetylacetone on the particle surface during stirring and sonication eliminates the appearance of large pores in the deposit and facilitates the formation of compact films.

The deposition yield can be calculated by the following equation, derived by Hemaker:[21]

$$m = f\mu CESt \quad (5)$$

where m (g) is the deposition yield, μ ($cm^2\ s^{-1}\ V^{-1}$) is the electrophoretic mobility, C (g/cm^3) is the concentration of solids in the suspension, S (cm^2) is the electrode area, E ($V\ cm^{-1}$) is the electric field, t (s) is the deposition time, and f is a dimensionless factor called the sticking factor, which takes into account the fact that not all moving particles will be deposited on the electrode ($f \leq 1$). When the concentration of solids and ions remains constant or does not change much, deposition at constant current will fit the linearity of eq 5. A constant deposition rate is a desirable factor for membrane fabrication, since a variable rate will give rise to different morphology in the direction of film growth. A membrane that is conformal and highly adhesive to the cathode and anode materials is mandatory for good performance of 3D microbatteries. Polyethyleneimine is known to be an inhibitor of crack propagation in electrophoretically deposited ceramic films.[23,25] In this work, the effect of PEI addition on membrane morphology and electrochemical properties has been studied. Figure 1 shows the deposit yields at 1.6 mA/cm^2 as a function of deposition time from binder-free and PEI-containing suspensions. EPD was carried out on pristine nickel substrate and on nickel that had been previously coated by $LiFePO_4$ cathode films. The curves represent the linear fit of the results, which show a constant deposition rate for all the samples. The calculated deposition-yield rates of the membrane are summarized in Table 1.

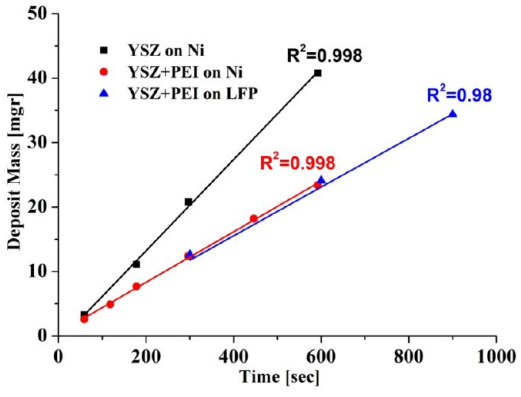

Figure 1. Plot of the mass of deposit as a function of deposition time.

Table 1. The Weight of the Membrane Electrophoretically Deposited on Ni and on LFP/Ni Substrates (as in Figure 1)

substrate	PEI content [% of YSZ weight]	Yield rate [$10^{-3}mgcm^{-2}s^{-1}$]
nickel	0	68.6
nickel	1.5	40.4
LFP on Ni	1.5	38.2

As can be seen in Figure 1, the deposition rate from a binder-free suspension is almost twice that of the rate from a suspension containing 1.5% PEI. A possible explanation of these data is as follows. Polyethyleneimine is a cationic polymer with highly branched globular structure. When PEI is dissolved in neutral or acidic aqueous solution, the imine groups of the chain are protonated (similar to NH_3/NH_4^+) and the macromolecule has a net positive charge. In ref 27, it was found that at pH 4−5 the degree of PEI ionization (α) is about 0.5−0.7. The electrostatic interaction between the neighboring ionized groups is very weak and is assumed to be negligible in the low-ionization region but becomes strong in the region of $\alpha > 0.4$. The strong electrostatic repulsion causes the PEI molecule to undergo transition from a compact coiled conformation to one that is stretched. In nonaqueous media, there is competitive adsorption between ionized PEI molecules and the protons generated in reactions 1−4 on the YSZ particles. While there is no direct evidence of the phenomenon, the partial substitution of absorbed protons by ionized PE is not impossible. Using FTIR, Wang and Gao[24] showed that PEI is anchored to ZrO_2 nanoparticles and that adsorption is accompanied by the formation of a ZrO_2/PEI interface complex. The authors suggest that hydrogen bonding and electrostatic attraction govern the mechanism of polymer adsorption. As a result of the formation of large "corona-like"-type micelles, the effective positive charge of the particle with adsorbed PEI is reduced. This causes deterioration of the deposition rate. On the other hand, steric repulsion of the micelles prevents their coagulation and the formation of rough films (see Figures 2 and 3).

In addition, a lower deposition rate might be associated with a high and continuously growing resistance of the deposit containing polymer, and of the suspension as well. The last factor might be due to the depletion of protons at the near-electrode surface, since these undergo reduction, impeded by the limited ion permeability through the porous ceramic deposit of high tortuosity.

As can be seen in Figure 1, the deposition rate from the PEI-containing suspension on LFP substrate is actually the same as that on nickel. We presume that, because of the high porosity and low resistivity of the carbon-modified $LiFePO_4$ film,[22] it does not impede the reduction of protons on the underlying nickel current collector.

Here we wish to emphasize that each batch of films (a, b, c) was deposited in sequence from a newly prepared solution. For all tests, the deposition rate remained constant even up to 10−15% YSZ depletion from the solution. This is a technological advantage, since many samples can be produced by EPD from the same suspension before its composition and the operating parameters of the process need to be corrected.

dx.doi.org/10.1021/jp305087h | J. Phys. Chem. B 2013, 117, 1577−1584

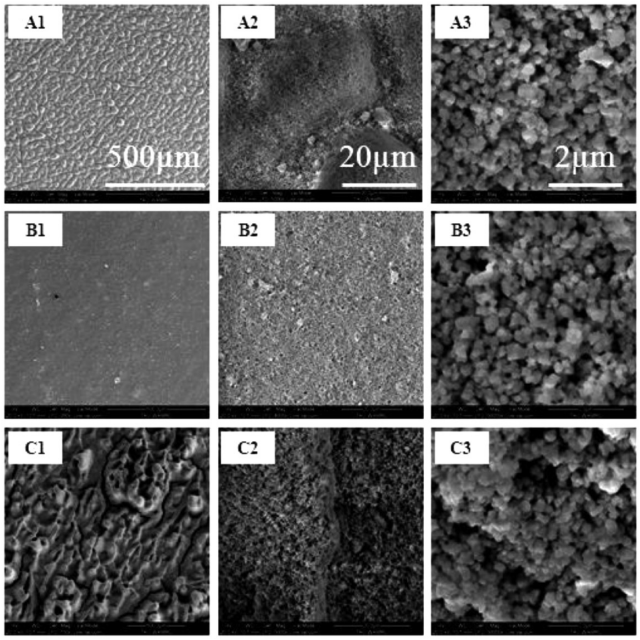

Figure 2. ESEM images of pristine and composite membrane. (A1−A3) pristine YSZ membrane on nickel; (B1−B3) PEI-modified YSZ membrane on nickel; (C1−C3) PEI-modified YSZ membrane on LFP.

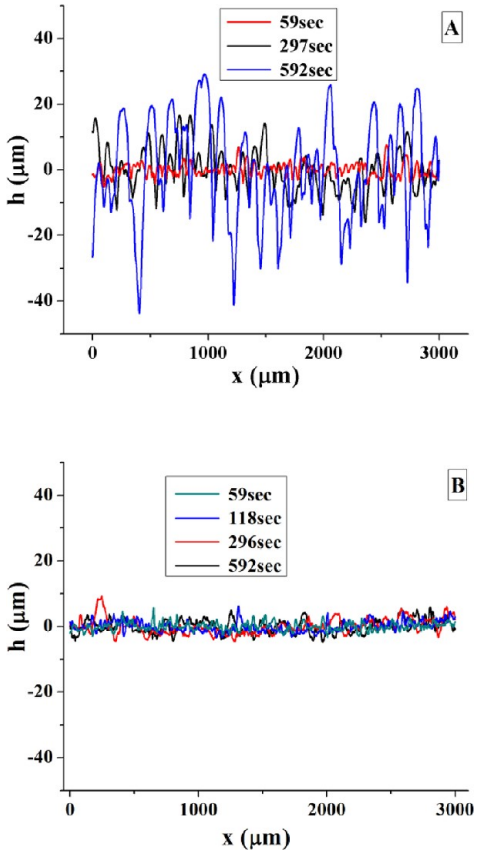

Figure 3. Plot of profilometer line scan (A) pristine YSZ film on nickel; (B) PEI-modified YSZ film on nickel.

Different characterization methods have been applied in order to find correlation between the properties of the film and the deposition parameters. Figure 2A1−A3 shows ESEM images at different magnifications of the membrane deposited on nickel from a PEI-free suspension. Parts B1−B3 and C1−C3 show the samples electrophoretically deposited from a PEI-containing suspension on nickel and LFP, respectively. The scales of the upper micrographs apply to the images below, as well. At high magnification, the morphology of the YSZ membrane appears to be similar for all samples. However, close inspection of the 2 μm scale micrograph of the PEI-modified ceramic membrane shows better separation of individual particles, the size of which, as determined by XRD, was about 200 nm. In low-magnification images, a large difference is observed. The roughness of the binder-free membrane is much greater than that of the sample deposited from a suspension containing PEI. A high degree of roughness can originate from the coagulation of the neat YSZ particles, while the PEI−ZrO_2 micelles seem to be more separated. Moreover, addition of PEI to the suspension improves the adhesion of the membrane to the substrate. The roughness of an electrophoretically deposited $LiFePO_4$ cathode according to the procedure developed by us previously[22] was about 10 μm. Examination of the ESEM images of the YSZ membrane deposited on LFP shows a similar roughness, which means that the membrane layer is conformal. This is a desired property for Li-ion batteries, since dendrite growth is sensitive to resistivity changes across the cell. A qualitative test of film adhesion was applied by scraping with the tip of a plastic pipet. The particle-to-substrate and particle-to-particle adhesion in the binder-free deposit was very weak; the film surface was very rough and the film was scraped easily in the form of a compact ceramic powder. This result is not surprising: when EPD is used for the manufacturing of ceramic components, a following step of high-temperature sintering is typically applied. For the preparation of Li-ion membrane, which is deposited directly on the cathode material, such heat treatment is not an option, since the cathode materials decompose at above 500 °C. On the other hand, the PEI−YSZ film could not be removed by scraping and the surface is much smoother. When an aggressive scraping test was carried out with stainless-steel tweezers, a large part of the deposit was removed as a continuous film and not as a powder. Such electrophoretically deposited films can be tested for mechanical strength and hardness.

To examine quantitatively the effect of PEI addition on the membrane structure, the lateral-thickness distribution of the YSZ-on-nickel films was measured by a profilometer. The standard deviation (STDV) of the results was used as a characteristic roughness factor. Typical data of the profilometer tests for different deposition times are presented in Figure 3.

For the binder-free YSZ membrane, the roughness increases with time to above 15 μm STDV for the 592 s deposition. For the PEI-modified YSZ membrane, the STDV is about 1.5 μm independent of the deposition time. The profilometer was also used to determine the thickness of the membrane. Since the area and weight have been measured, evaluation of the real density of the film can be obtained and the porosity of the film can be calculated. The PEI:YSZ ratio in the deposited membrane estimated from the TGA tests (not shown here) was 2:98(w/w). The density of PEI-modified YSZ composite material was 5.58 g/cm^3 (compared to 5.68 g/cm^3 in the case of pure ceramics). On the basis of the above data, the estimated porosity of the membrane is 54 ± 5%. The dependence of the film thickness on the deposition time was analyzed in an effort to determine if the porosity across the film is uniform. As can be seen from Figure 4, the thickness of the film is linear with time, indicating homogeneous pore distribution along the

dx.doi.org/10.1021/jp305087h | J. Phys. Chem. B 2013, 117, 1577−1584

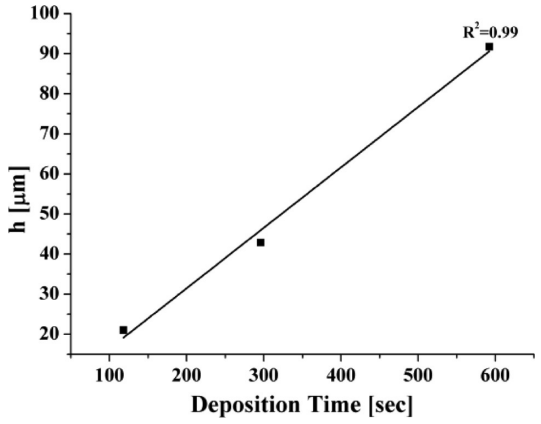

Figure 4. Film thickness vs deposition time for PEI-modified YSZ membrane on nickel.

direction of film growth. Voltage vs time deposition curves (Figure 5) correlate with the data presented so far. As

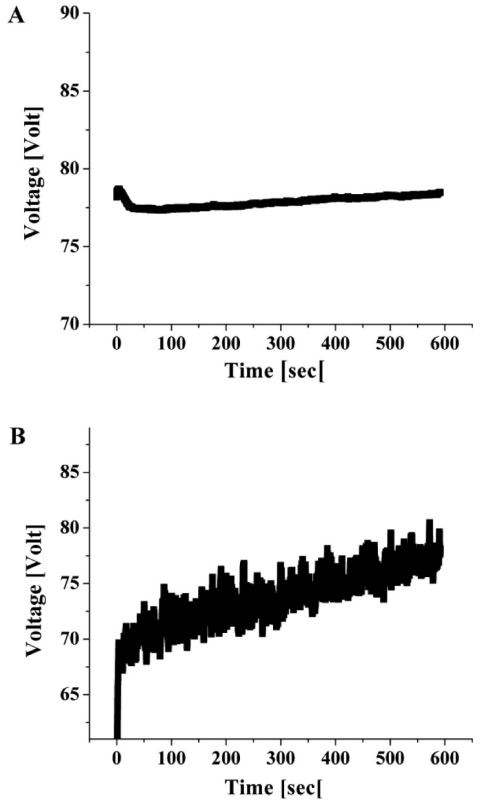

Figure 5. Voltage vs time deposition curves: (A) pristine YSZ membrane on nickel; (B) PEI-modified YSZ film on nickel.

mentioned in the Experimental Section, the voltage was measured between the counter and working electrodes of the cell. The specific resistivity of the growing membrane is higher than that of the suspension; therefore, the voltage gradually increases during the EPD process. The slope of the $V-t$ curve of the PEI-free membrane is more pronounced (6.5 times that of the polymer-modified membrane). This is in agreement with the higher deposition rate. Moreover, the EPD of the modified membrane is characterized by a much smoother profile of the deposition curve (Figure 5A). Spikes observed in Figure 5B can be related to the nonhomogeneous macroscopic morphology of the pristine YSZ membrane and poor adhesion to the substrate and between ceramic particles. This may cause local resistivity changes that are reflected in the strong aperiodic voltage fluctuations. Increase of the PEI content, up to 10%(w/w) in the suspension, was followed by a significant increase in the voltage during the EPD process, but the thickness of the films did not change by much. We attribute this observation to the increased viscosity of the suspension rather than to the additional adsorption of PEI molecules on the surface of the ceramic particles. This is in agreement with the TGA tests, in which it was found that the concentration of PEI shows little change in the samples deposited from suspensions with 4, 6, and 10% PEI.

TOFSIMS analysis was carried out with the aim of determining the lateral and bulk distribution of the polymer in the composite films. Mass spectra were obtained in order to determine the elemental and molecular species on the top and bottom surfaces of the membrane separated from the nickel substrate (Figure 6). The most characteristic fragments associated with PEI have a $[m/z]$ ratio of 30 and 44, which relate to CH_4N and C_2H_6N species, respectively. The ion counts of the fragments appear to be almost the same for both surfaces, indicating homogeneous distribution of PEI across the film. Positive-ion TOFSIMS images were acquired from a 1 μm diameter area in order to visualize the lateral distribution of species. The results are presented in Figure 6C and D. Both Zr^+ and $C_2H_6N^+$ species show homogeneous allocation and complete mixing of zirconia and PEI.

Electrochemical-impedance spectroscopy (EIS) was used to estimate the ionic conductivity of an electrophoretically deposited composite membrane soaked in a commercial $LiPF_6$ EC:DEC electrolyte. The results are presented in Table 2, with comparison to the commercial Celgard separator.

The apparent "effective" conductivity of the electrolyte (σ_{eff}) trapped in the composite EPD membrane was estimated with the use of the Bruggeman relation.[28,29] The "effective" conductivity is actually the bulk conductivity of the liquid electrolyte in porous media.

$$\sigma_{eff} = \varepsilon^{\alpha}\sigma_0 \tag{6}$$

where σ_0 is the conductivity of the liquid phase alone, ε is the void-volume fraction of the porous electrode or separator filled with electrolyte, and α is the Bruggeman exponent. Other researchers approximate the effective electrolytic conductivity of a porous network by the MacMullin number N_M according to eq 7:

$$N_M = \sigma_0/\sigma_{eff} \tag{7}$$

The MacMullin number reflects the decrease in conductivity (increase in resistivity) of a liquid electrolyte caused by a porous separator. N_M is actually the ratio of the resistivity of the separator filled with electrolyte to the resistivity of the electrolyte alone. Comparing eqs 6 and 7 yields

$$N_M = \varepsilon^{-\alpha} \tag{8}$$

Abraham[30] suggested another relationship between the MacMullin number and porosity by introducing a tortuosity parameter, τ, i.e.,

$$N_M = \tau^2/\varepsilon \tag{9}$$

By combining eqs 8 and 9, it is easy to transform τ values[9] to formal Bruggeman exponents according to

dx.doi.org/10.1021/jp305087h | J. Phys. Chem. B 2013, 117, 1577−1584

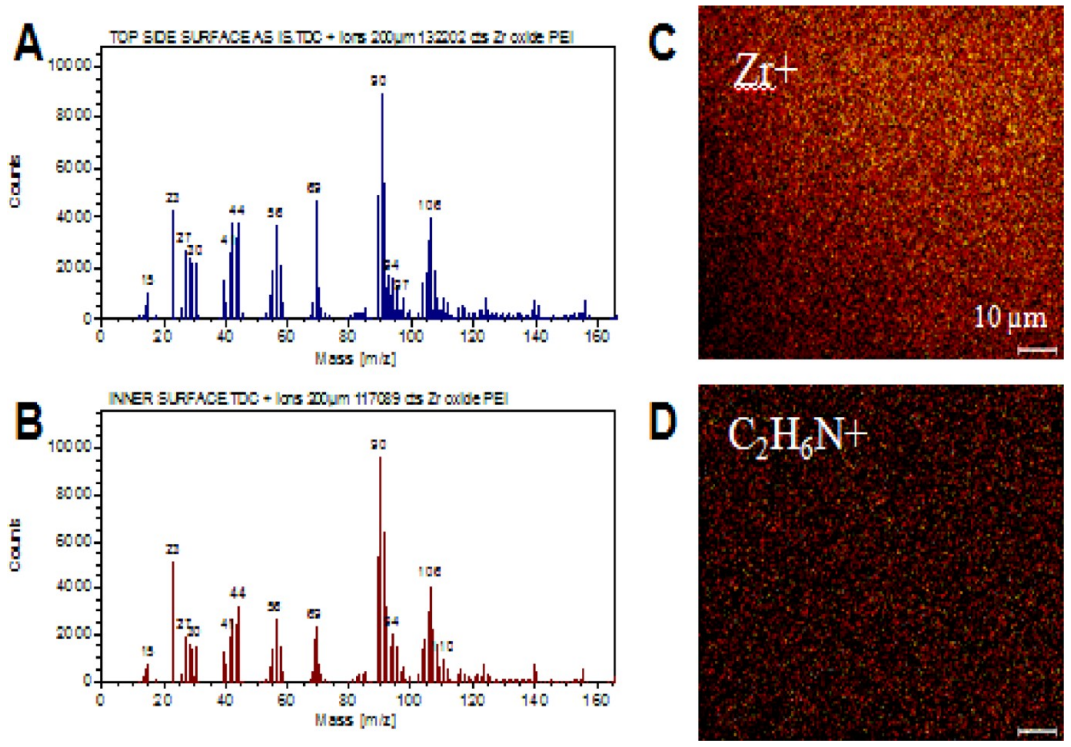

Figure 6. TOFSIMS mass spectra and surface images: (A) mass spectrum of the top surface; (B) mass spectrum of the top surface; (C) lateral distribution of Zr^+ ions; (D) lateral distribution of $C_2H_6N^+$ ionic species.

Table 2

separator	L (μm)	porosity, ε (%)	effective conductivity, σ_{eff} ($S \cdot cm^{-1}$)	N_m	τ
ZrO_2	40	54	1.7×10^{-3}	4.6	1.6
CG 2400	25	40	9.2×10^{-4}	8.6	1.9

$$\alpha = 1 - 2\log(\tau)/\log(\varepsilon) \quad (10)$$

Doyle et al. state[31] that, for Celgard membranes, the experimental data are compatible with eq 5 only if the formal Bruggeman exponent (α) is adjusted to values varying from 3 to 4.5. For Celgard 2400, the values of ε, N_M, and α are as follows: 0.37, 15.7, and 2.8. For Celgard 2500, these parameters are 0.55, 8.5, and 3.6, respectively.[31]

The conductivity of the baseline $LiPF_6$:EC:DEC liquid electrolyte (σ_0) is 7.9 mS cm^{-1} at 25 °C.[1] From eq 6, one finds that a better fit of the effective conductivity of a composite PEI–YSZ membrane prepared by EPD is obtained by using an exponent close to 2.5 in the Bruggeman formula. The MacMullin number of the porous YSZ membrane with higher effective conductivity is almost half that of Celgard 2400. The tortuosity makes it possible to take into account the impact of the complexity of the porous structure of the membrane on the conductivity. If we combine eqs 7 and 9, the tortuosity of membrane can be approximated by eq 11:

$$\tau = (\sigma_0 \varepsilon/\sigma_{eff})^{1/2} \quad (11)$$

The calculated tortuosity value of the modified EPD membrane (Table 2) is close to that of commercial Celgard (CG 2400).

L is the membrane thickness measured by the profilometer. The porosity (ε) of the composite polymer–ceramic membrane has been calculated from the total volume and the membrane weight as described above. σ_{eff} is the effective conductivity, calculated from the total resistance of the membrane (Ω) as measured by EIS at 5×10^6 Hz.

As can be seen from Table 2, the effective conductivity of the composite membrane is higher than that of the CG2400. This result can be attributed to the high porosity, good wettabilty, and electrolyte retention, typical of ceramic separators.[9]

Figure 7 presents a comparison between the cycling performance of the cell containing a YSZ–PEI separator

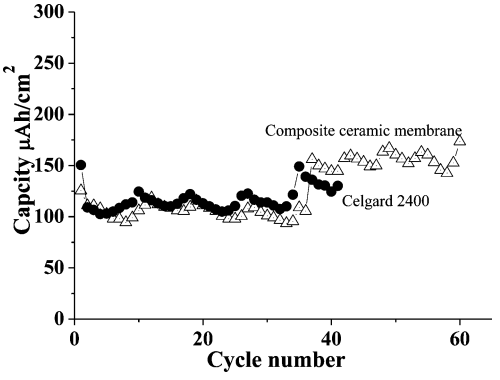

Figure 7. Cycling life plots of Li/$LiFePO_4$ cells with Celgard and PEI-modified YSZ membrane.

deposited on an LFP cathode and the cell with Celgard. The cells were initially charged at a constant voltage of 3.6 V for 30 min and then cycled over the voltage range 2.8–3.5 V. The LFP cathode was prepared by EPD according to the procedure described in ref 22. Since the process of cathode deposition was in the initial stages of development and the cycling procedure had not yet been finalized, an additional half-hour-long charge was applied to the system after the 34th cycle. As evidenced by the plots of capacity vs cycle number, the discharge capacity of

dx.doi.org/10.1021/jp305087h | J. Phys. Chem. B 2013, 117, 1577–1584

the cell with a modified YSZ membrane is almost the same and even slightly higher than that of the cell with Celgard. Moreover, after the second charge, the composite-membrane cell reached a stable capacity of about 150 mAh/g, which is close to the performance of commercial cells with LFP cathodes. The comb shape of the curve is caused by daily temperature fluctuations in the laboratory. A maximum capacity was always reached at about 1:00 p.m., the hottest hour of the day, while minimum capacity is obtained at approximately 5:30 a.m., which is the coldest hour.

Figure 8 shows dq/dv charge/discharge curves of both cells. The voltage plateaus at about 3.45 and 3.4 V appear as peaks in

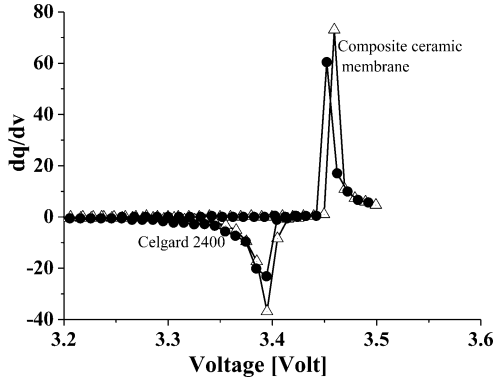

Figure 8. dq/dv curves of the charge/discharge of Li/$LiFePO_4$ cells (cycle 18) with Celgard and PEI-modified YSZ membrane.

the plots for charge and discharge processes, respectively. The charge/discharge overpotential of the cells is almost the same. These data indicate high compatibility of the EPD composite ceramic membrane with an $LiFePO_4$ cathode and Li anode.

Electrophoretic deposition of a modified composite membrane on the 3D perforated silicon substrate was carried out with the use of the homemade deposition setup, which provides continuous flow of the suspension through the microchannels. The thickness of the substrate was 400 μm, the diameter of a single channel was 50 μm, and the interhole spacing was 20 μm. The perforated substrates were prepared with the use of the deep reactive ion-etching (DRIE) method by Philips Research Laboratories. Planar (Figure 9A) and cross-sectional SEM micrographs at different magnifications (Figure 9B–E) of the PEI-modified YSZ film deposited on the gold-coated, perforated silicon chip show that the morphology of the 3D deposit inside long narrow channels is similar to that obtained on the planar substrates. A conformal thin-film LFP coating was obtained throughout the in-chip microchannels. Figure 10 shows a tilted cross-sectional view of the fractured, perforated silicon chip, coated by three consecutive layers of Au, $LiFePO_4$, and ZrO_2–PEI membrane. As can be seen from Figure 10, the LFP cathode and membrane were too thick and partially plugged the microchannels. Optimization of the EPD processes for the preparation of 3D thin-film microbattery layers confined in high-aspect-ratio microchannels is underway and will be presented in forthcoming publications.

CONCLUSIONS

We have found that the EPD process of pristine and composite ceramic membranes follows a simple linear relationship between time and mass of the deposit for the tested ranges of values of the relevant parameters. Addition of PEI polymer

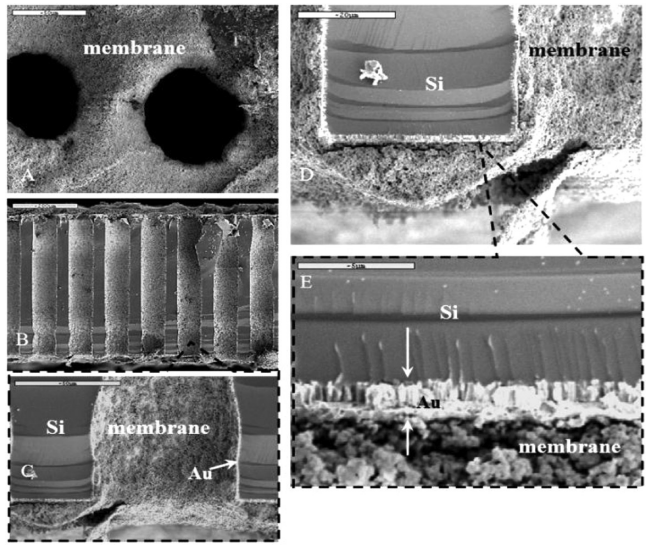

Figure 9. ESEM images of PEI-modified YSZ membrane deposited on gold-coated perforated silicon chip.

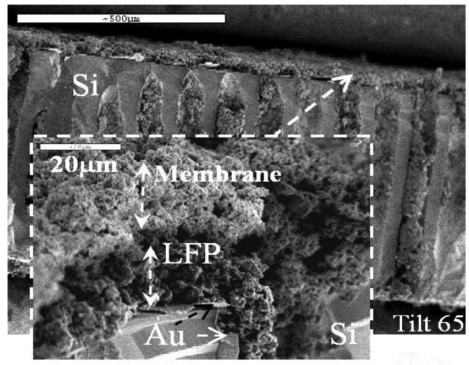

Figure 10. Tilted cross-sectional ESEM view of the fractured perforated Si chip coated by three consecutive layers of Au, $LiFePO_4$, and YZS–PEI membrane.

to the suspension improved film adhesion to planar nickel and 3D-perforated silicon substrates and reduced the film roughness to less than 2 μm, even at long deposition times. TOFSIMS spectra and positive-ion-species images showed homogeneous lateral and depth distribution of the polymer binder in electrophoretically deposited composite films. The ionic conductivity of the porous composite ZrO_2-based membrane filled by $LiPF_6$:(EC/DEC) liquid electrolyte is higher than that of commercial battery separators. The cycleability and charge/discharge behavior of planar $LiFePO_4$/(ZrO_2–PEI) $LiPF_6$ EC:DEC/Li cells are similar to those of the cells with commercial Celgard membrane. Conformal coating of the 2D and 3D electrode materials by a thin-film ceramic separator is beneficial for high-power battery operation. This separator is able to prevent high-temperature thermal runaway and significantly improve battery safety.

AUTHOR INFORMATION

Corresponding Author

*E-mail: ronihada@tau.ac.il (R.H.); golod@post.tau.ac.il (D.G.).

Notes

The authors declare no competing financial interest.

■ ACKNOWLEDGMENTS

The authors thank Philips Research Laboratories for preparation of the perforated silicon substrates in the frame of EU FP7 project SUPERLION (www.superlion.eu).

■ REFERENCES

(1) Linden, D.; Reddy, T. *Handbook of Batteries*, 3rd ed.; McGraw-Hill: 2002.
(2) Garche, J. *Electrochemical Power Sources*, 1st ed.; Elsevier: 2009.
(3) Yoshio, M.; Brodd, R.; Kozawa, A. *Lithium-Ion Batteries*; Springer: 2009.
(4) Long, J. W.; Dunn, B.; Rolison, D. R.; White, H. S. *Chem. Rev.* **2004**, *104*, 4463−4492.
(5) Roberts, M; Johns, P.; Owen, J.; Brandell, D.; Edstrom, K.; Enany, G. E.; Guery, C.; Golodnitsky, D.; Lacey, M.; Lecoeuret, C.; et al. *J. Mater. Chem.* **2011**, *21*, 9876−9890.
(6) Golodnitsky, D.; Nathan, M.; Yufit, V.; Strauss, E.; Freedman, K.; Burstein, L.; Gladkich, A.; Peled, E. *Solid State Ionics* **2006**, *177*, 2811−2819.
(7) Golodnitsky, D.; Nathan, M.; Yufit, V.; Shechtman, I.; Ripenbein, T; Strauss, E.; Menkin, S.; Peled, E. *J. Power Sources* **2006**, *153*, 281−287.
(8) Golodnitsky, D.; Nathan, M.; Yufit, V.; Strauss, E.; Ripenbein, T; Shechtman, I.; Menkin, S.; Peled, E. *J. Microelectromech. Syst.* **2005**, *14* (5), 879−885.
(9) Zhang, S. S. *J. Power Sources* **2007**, *164*, 351−364.
(10) Zhang, S. S.; Xu, K.; Jow, T. R. *J. Power Sources* **2005**, *140*, 361−364.
(11) Xiang, H.; Chen, J.; Li, Z.; Wang, H. *J. Power Sources* **2011**, *196*, 8651−8655.
(12) Kim, M.; Nho, Y. C.; Park, J. H. *J. Solid State Electrochem.* **2010**, *14*, 769−773.
(13) Fukada, Y.; Nagarajan, N.; Mekky, W.; Bao, Y.; Kim, H. S.; Nicholson, P. S. *J. Mater. Sci.* **2004**, *39*, 787−801.
(14) Besra, L.; Liu, M. *Prog. Mater. Sci.* **2007**, *52*, 1−61.
(15) Van der Biest, O. O.; Vandeperre, L. J. *Annu. Rev. Mater. Sci.* **1999**, *29*, 327−352.
(16) Ferrari, B.; Moreno, R. *J. Eur. Ceram. Soc.* **2010**, *30*, 1069−1078.
(17) Zhitomirsky, I. *Adv. Colloid Interface Sci.* **2002**, *97*, 279−317.
(18) Tang, F.; Uchikoshi, T.; Ozawa, K.; Sakka, Y. *J. Eur. Ceram. Soc.* **2006**, *26*, 1555−1560.
(19) Grinis, L.; Dor, S.; Ofir, A.; Zaban, A. *J. Photochem. Photobiol., A* **2008**, *198*, 52−59.
(20) Dor, S.; Ruhle, S.; Ofir, A.; Adler, M.; Grinis, L.; Zaban, A. *Colloids Surf., A* **2009**, *342*, 70−75.
(21) Hamaker, H. C. *Trans. Faraday Soc* **1940**, *35*, 279−287.
(22) Mazor, H.; Golodnitsky, D.; Burstein, L.; Gladkich, A.; Peled, E. *J. Power Sources* **2012**, *198*, 264−272.
(23) Tang, F.; Uchikoshi, T.; Ozawa, K.; Sakka, Y. *J. Eur. Ceram. Soc.* **2006**, *26*, 1555−1560.
(24) Wang, J.; Gao, L. *J. Colloid Interface Sci.* **1999**, *216*, 436−439.
(25) Zhitomirsky, I. *Surf. Eng.* **2004**, *20*, 43−47.
(26) Koura, N.; Tsukamoto, T.; Shoji, H.; Hotta, T. *Jpn. J. Appl. Phys.* **1995**, *34*, 1643−164.
(27) Zhu, X.; Tang, F; Suzuki, T. S.; Sakka, Y. *J. Am. Ceram. Soc.* **2003**, *86* (1), 189−91.
(28) Bruggeman, D. A. G. *Ann. Phys.* **1935**, *24*, 636−679.
(29) Meredith, R. E.; Tobias, C. W. *Adv. Electrochem. Electrochem. Eng.* **1962**, *2*, 15−47.
(30) Abraham, K. M. *Electrochim. Acta* **1993**, *38*, 1233−1248.
(31) Doyle, M.; Newman, J.; Gozdz, A.; Schmutz, C. N.; Tarascon, J.-M. *J. Electrochem. Soc.* **1996**, *143*, 1890−1903.